



# **Within the Coesite Stability Field - a HP-Study**

Julia Langer, Christian-Albrechts-University of Kiel, Germany

September, 2015

Supervised by Dr. Norimasa Nishiyama, MSc Eleonora Kulik & MSc Nico Gaida

## **Abstract**

This study has been about the mineral phase coesite, which is a high pressure  $\text{SiO}_2$  polymorph.

After synthesizing various samples with a multi-anvil press, measurements were carried out: Besides using an XRD to determine their structure, also the hardness, the toughness and the density of the samples were measured. All this obtained data was used to receive a better understanding on the mechanical properties of the synthesized samples and will be presented in the following report.

## **Table of content**

1. Introduction

2. Starting Material

3. Methods

3.1. Multi-anvil

3.2. XRD

3.3. Density Measurements

3.4. Hardness & Toughness Measurements

4. Experiments

5. Results

5.1. XRD – Results

5.2. Density Measurement Results

5.3. Hardness Measurement Results

5.4. Toughness Measurement Results

6. Discussion

References

## 1. Introduction

Coesite is a high pressure  $\text{SiO}_2$  polymorph, which means, it has the same chemical composition but differs in structure to the stable phase quartz at ambient pressure and temperature. It is stable above 2-4 GPa, below 8-10 GPa and below about 2600°C (Figure 1).

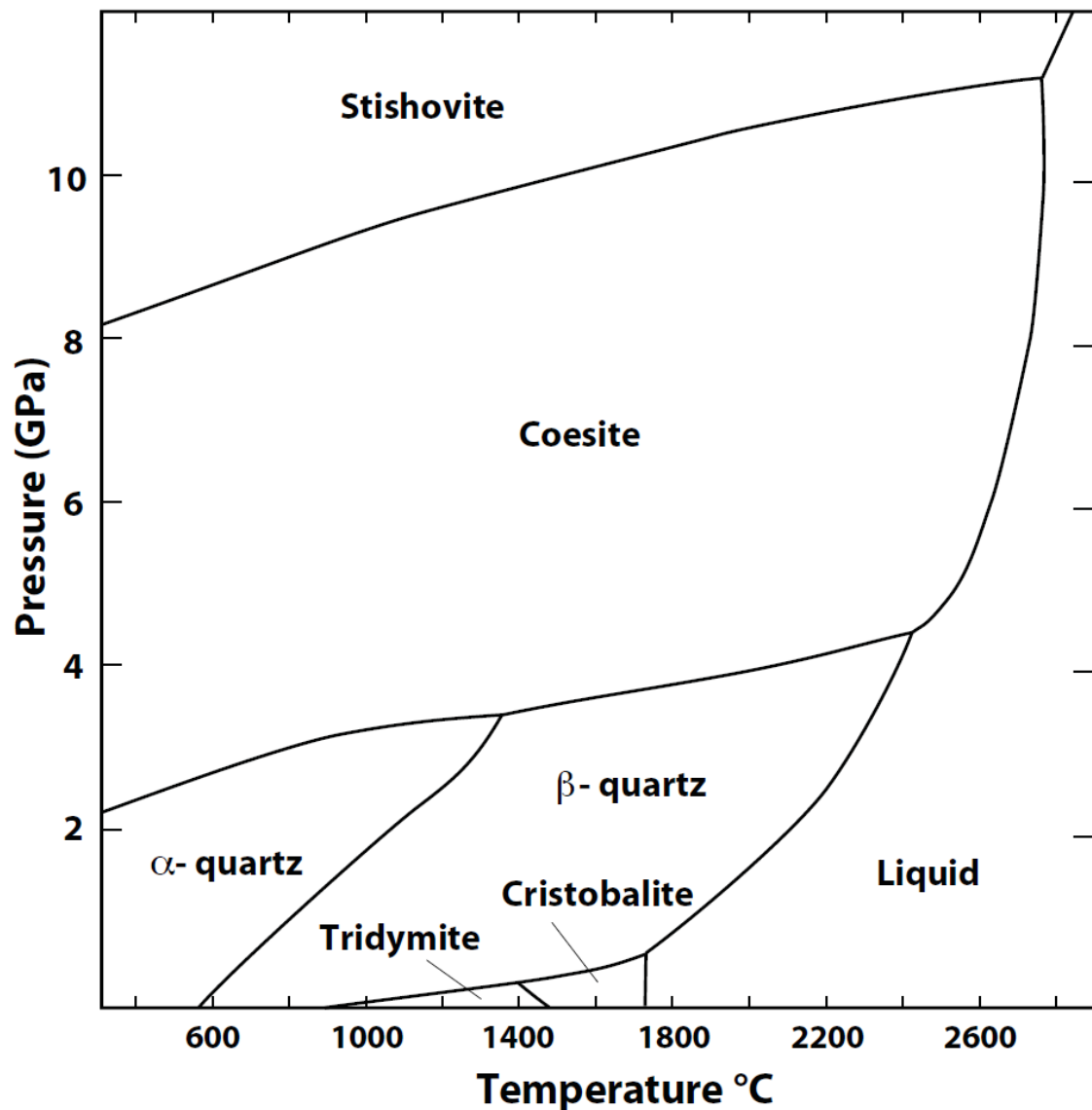


**Fig. 1:** P-T-diagram of  $\text{SiO}_2$ . [Swamy et al., 1994]

This mineral phase was first discovered by Coes in 1953 and later observed by Chao et al., 1960, in a natural sample of an impact breccia from the Meteor Crater, Arizona. Nowadays coesite is an indicator for high pressure rocks. It is related to meteorite impacts due to shock-induced metamorphism or occurs as mineral inclusion within terrestrial, exhumed, metamorphosed or mantle derived rocks [e.g. Smyth & Hatton, 1977; Chopin, 1984; Parkinson, 2000].

Coesite however does not have a distinct short-range order; it rather undergoes several metastable phase transitions during compression, which is described by Černok et al., 2014. These metastable phase transitions within the stability field of coesite are due to the relatively strong Si-O bonding in silica crystals. Therefore the kinetic barrier of coesite in general is rather high, which implies the metastability of coesite at ambient pressure and temperature.

It is generally accredited that the mineral phase silica has a much more complex phase diagram than shown in Figure 1, which is due to the fact of the various possibilities of arranging the basic module: a fourfold coordinated silicon atom surrounded by oxygen atoms. This leads to a variety of physical properties. Therefore silica, which is highly abundant on earth, gives rise to the material scientific research on its specific properties under various conditions.

## 2. Starting Material

The starting material within all operated experiments during this study was highly pure amorphous SiO<sub>2</sub> with a hydrogen content of less than 1ppm. It was purchased from OHARA QUARTZ CO., LTD. with the product name SK-1310 as a rod with a diameter of 4 mm. The physical properties of this SiO<sub>2</sub> glass are tabulated in Table 1.

**Tab. 1:** Physical Properties of the product SK-1310 from OHARA QUARTZ CO., LTD.. [Material Master Data Sheet of SK1310 from OHARA Corporation [1]]

Density	2.20 g/cm <sup>3</sup>
Coefficient of thermal expansion	5.5x10 <sup>-7</sup> 1/K
Young's module	71.6 GPa
Torsional Rigidity	31.4 GPa
Softening Point	1700 °C
Poisson's Ratio	0.17
Annealing Point	1160 °C
Compression Strength	1.1 GPa
Strain Point	1060 °C
Bending Strength	69 GPa
Tensile Strength	55 GPa
Specific Heat (26°C)	0.74 kJ/kg · K
Vickers Hardness	8.8~10.1 GPa

This starting material was chosen for this experimental series to reduce the crystallization potential at impurity atoms within the glass.

### 3. Methods

During this study different methods were used to analyze the samples, which were synthesized within a multianvil press. The following subchapters will describe the exact systematic approach.

#### 3.1. Multianvil Press

At DESY, Hamburg, a Kawai-type high pressure apparatus of the model LPR 1000-400/50 built by the Max Voggenreiter GmbH is installed (Figure 2). A so called multianvil press is a device to synthesize samples at high pressures and high temperatures if applicable.

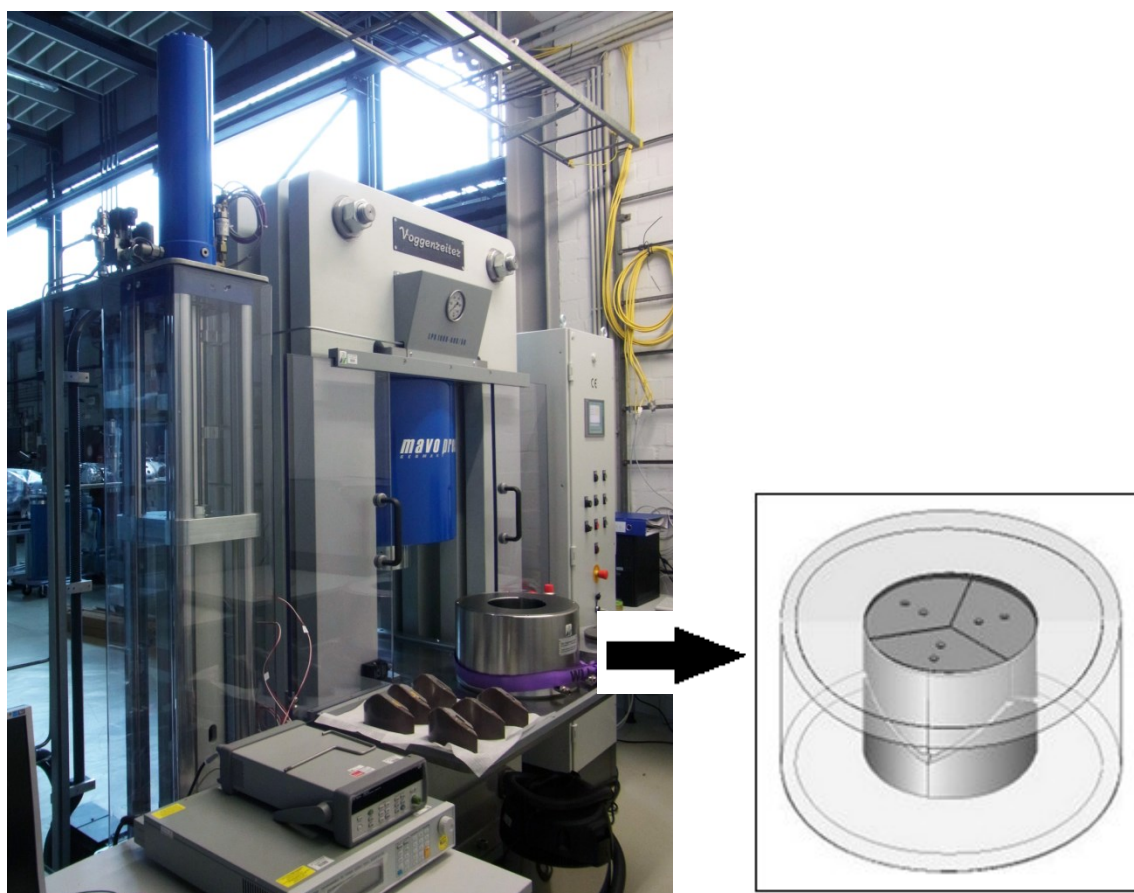


**Fig.2:** Multianvil press with a Walker module including a Kawai-type cell assembly installed at Photon Science, DESY.

The setting persists of a hydraulic oil press with a maximum pressure range up to 700 bar and a Walker module for a Kawai-type anvil assembly. Thus there is a cylindrical steel support ring with six steel wedges, which conduct the applied pressure from six sides onto a cubic assembly of eight tungsten-carbide anvils. The cubic assembly of the eight anvils exhibits an octahedral-shaped cavity with certain truncation edge lengths (TEL) in their middle. This cavity is filled with a 5%  $\text{Cr}_2\text{O}_3$  doped  $\text{MgO}$ -octahedron representing the essential pressure medium, which contains the capsule assembly including the sample. This assembly consists of various parts with a certain assembling design, which is both shown in Figure 3 [Walker et al., 1990, Frost et al., 2004].

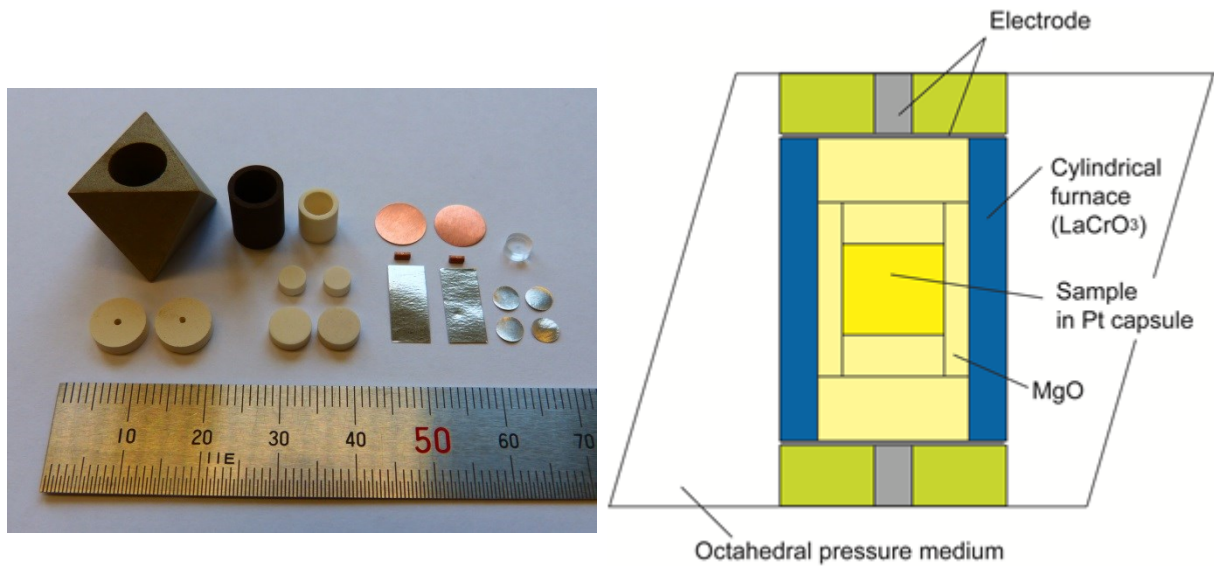


**Fig.3: Left:** Parts for the assembly of the octahedral pressure medium. **Right:** Design of cell assembly within the MgO-octahedron.

In Table 2 the exact parameters of the manufactured parts of the 18/11 cell assembly are given.

**Tab. 2:** Part parameters of the 18/11 cell assembly.

Part	Outer Diameter	Inner Diameter	Height
MgO-Octahedron	-	8 mm	-
ZrO <sub>2</sub> (2x)	8 mm	1 mm	2.25 mm
Cu-Discs (2x)	7.95 mm	-	1 mm
Cu-Electrodes (2x)	1 mm	-	2.25 mm
LaCrO <sub>3</sub>	8 mm	6 mm	10 mm
MgO-Cylinder	6 mm	4.3 mm	6 mm
MgO-Outer Parts (2x)	6 mm	-	2 mm
MgO-Inner Parts (2x)	4.05 mm	-	2 mm
PI-Discs (4x)	3.95 mm	-	2x 0.5 mm
PI-Outer Cylinder (Foil)	<b>Length:</b> 13 mm	<b>Thickness:</b> 0.5 mm	5.9 mm
PI-Inner Cylinder (Foil)	<b>Length:</b> 12.5 mm	<b>Thickness:</b> 0.5 mm	5.9 mm
Sample	4 mm	-	1.8 mm

To determine the pressures and the temperatures within a small error, pressure as well as temperature calibrations have to be performed in pre-experiments due to pressure-fixed points of phase transitions and thermocouple measurements. In this case the pressure calibration was done using Bi, ZnTe and ZnS as pressure-calibration-mediums due to their well know phase transition pressure points at ambient temperature (Figure 4). The temperature calibration was carried out using thermocouples with W<sub>0.95</sub>Re<sub>0.05</sub>-W<sub>0.74</sub>Re<sub>0.26</sub> alloys. The voltage measurements of these thermocouples were then recalculated to temperature differences and with the ambient temperature as a reference value the temperature within the cell assembly could be estimated within a small error margin (Figure 5).

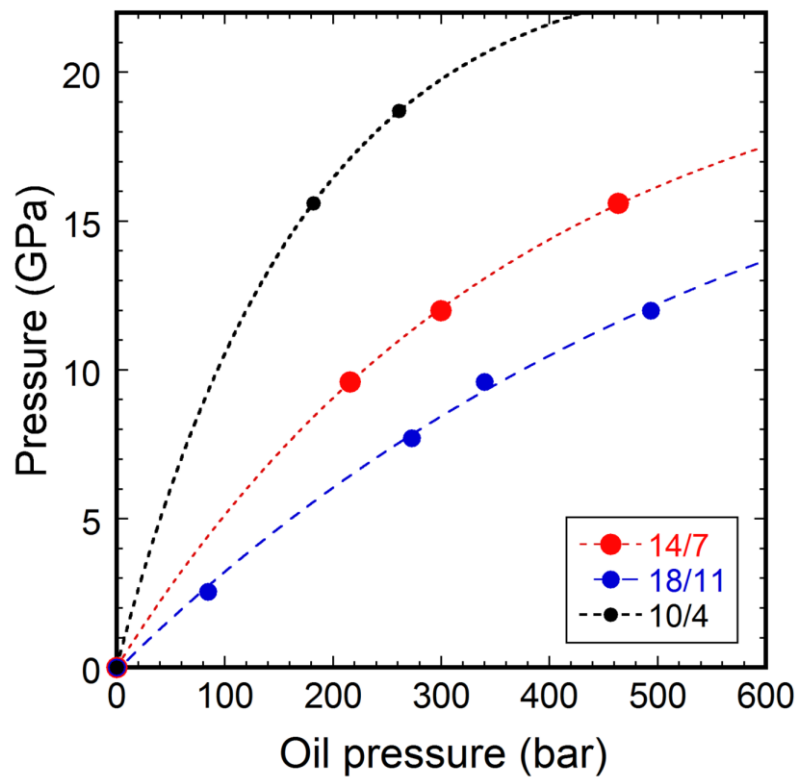


**Fig.4:** Diagram of pressure calibration curves at ambient temperature.

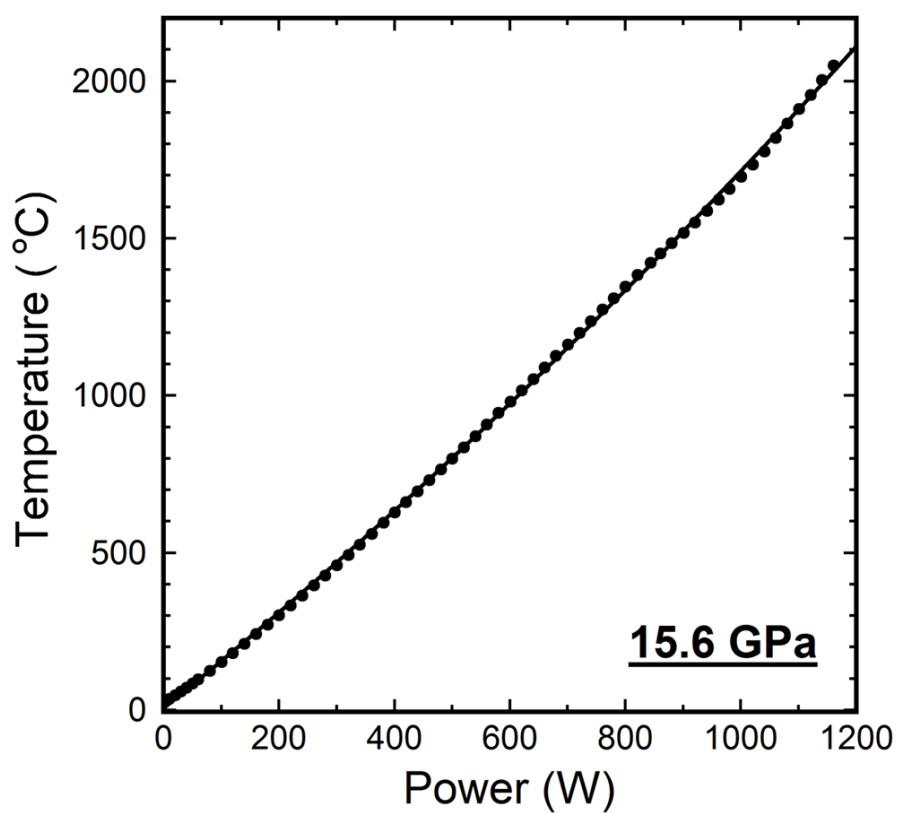


**Fig.5:** Diagram of temperature calibration curve at 15.6 GPa.

### 3.2. XRD

The X-ray diffraction measurements were carried out with an X-ray diffractometer Rigaku MiniFlex including a  $\text{CuK}\alpha$  – source with a wavelength of 0.15418 nm. Due to the selected diffraction of X-rays on the 3-dimensional lattice mesh of crystals and their distinct unit cells data on the crystal structure of single crystals, powder or bulk samples can be obtained. This method is determined by the constructive and destructive interference of electromagnetic waves diffracting on matter, which is stated within the Bragg and the Laue equations as well as in general diffraction theory. The general, internal setup of an XRD is shown in Figure 6.

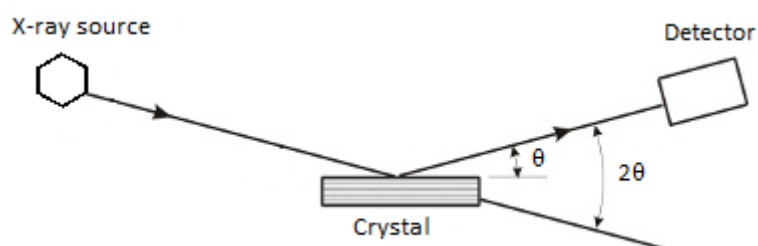


**Fig.6:** Scheme of the general, internal setup of an X-ray diffractometer.

### 3.3. Density Measurements

The density measurements are based on the principle of Archimedes and were carried out with a special setup incorporated within a Sartorius CPA 225D balance (Figure 7). The used medium to measure the exact density within a small error was 99.8% anhydrous Toluene,  $\text{C}_6\text{H}_5\text{CH}_3$ . Calibration runs are performed with a  $\text{SiO}_2$ -glass with the known density of  $2.2 \text{ g/cm}^3$ . Used Indentation loads were 100g, 200g and 500g.

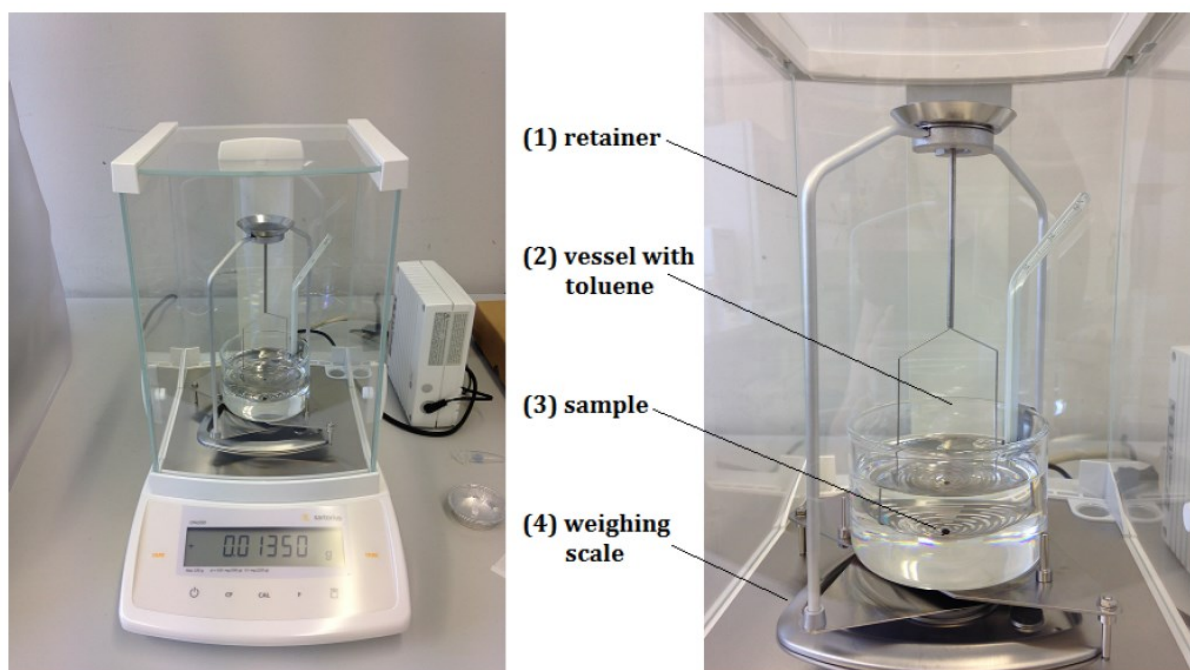


**Fig.7:** Setup for density measurements. [Gaida, 2014]



The density due to the Archimedes method is measured by weighing the sample within the air and weighing the sample in the liquid. This is done 10-times to receive a decent average value. The average density is then calculated as follows:

$$\rho = \frac{\rho_{toluene} \cdot m_{air}}{m_{air} - m_{liq}}$$

However the density of the liquid toluene is temperature dependent and therefore has to be regarded as follows:

$$\rho_{toluene} = 0.8852 / \frac{g}{cm^3} - 0.0009 \cdot T/^{\circ}C$$

### 3.4. Hardness & Toughness Measurements

There are several possibilities to measure the hardness and toughness of a material. In this study the Knoop Hardness Test with a Mitutoyo Hardness Testing Machine MicroWizard as well as the Vickers Indentation Fracture Test (VIF) with a Mitutoyo Hardness Testing Machine HV was carried out. These methods are about penetrating the sample surface with a pyramidal-shaped diamond (Figure 8). The requirements on the samples are a flat and smooth surface without impurities to avoid falsification of the test results.

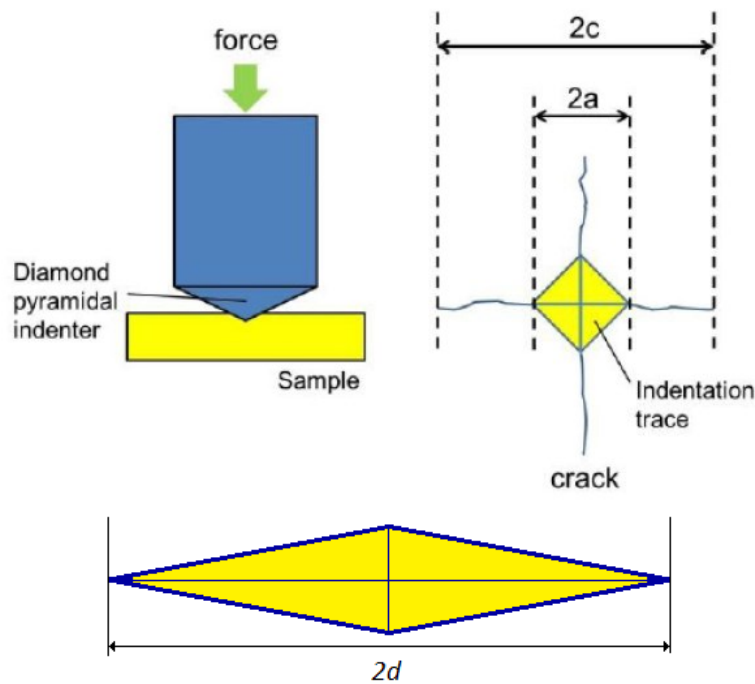


**Fig.8:** Scheme of Vickers Indentation Fracture Test and respectively Knoop Hardness Test. The distances  $2a$  and  $2c$  shown in the middle were measured during VIF test. The length of  $2a$  was recalculated to the Vickers hardness and the length of  $2c$  to the Vickers fracture toughness. The length of  $2d$  was recalculated to the Knoop hardness. [Modified after Gaida, 2014]

The Vickers hardness is calculated via the length of the penetration diagonal as follows:

with  $H$  as Vickers hardness in  $GPa$ ,  $F$  as indentation force in  $N$ ,  $L$  as the indentation load in  $kg$ ,  $g$  as gravitational acceleration in  $ms^{-2}$ ,  $\langle 2a \rangle$  as the average indentation diagonal in  $\mu m$  (Figure 8) and  $\phi = 136^\circ$  as apex-angle of Vickers pyramid in  $^\circ$ .

$$H = 2 \sin(\phi) \cdot \frac{gL}{\langle 2a \rangle^2} = 1854.4 \cdot \frac{F}{\langle 2a \rangle^2}$$

The Vickers fracture toughness is calculated via the length of the propagated fractures as follows:

$$K_{Ic} = \xi \left( \frac{E}{H} \right)^{1/2} \cdot \chi^{-3/2}$$

with  $K_{Ic}$  as the indentation fracture toughness in  $MPa \sqrt{m}$ ,  $c$  as the crack radius in  $\mu m$ ,  $\xi$  as geometry factor, which is described by Anstis et al. 1981 with the value of 0.016,  $E/H$  as the relation between modulus and hardness and  $\chi$  as a proportionality constant defined by

$$\chi = \frac{c}{F^{3/2}}$$

with  $c$  as average indentation fracture length in  $\mu m$  (Figure 8) and  $F$  as indentation force in  $N$  [Cook & Pharr, 1990].

The Knoop hardness is calculated via the length of the bigger penetration diagonals follows [Chuenarrom et al., 2009]:

$$HK = 14230 * \frac{F}{(2d)^2}$$

with  $HK$  as Knoop hardness in  $GPa$ ,  $F$  as indentation load in  $kg$  and  $d$  as the average diagonal in  $\mu m$ .

## 4. Experiments

During this study several synthesis experiments were carried out with the multianvil press installed at Photon Science DESY, Hamburg. Overall there were six experiments at 8 GPa and different temperatures from 800°C - 1600°C, which were collected for a gradual experimental series. Another experiment was conducted at 20 GPa and ambient temperature as contrast sample. All basic parameters of the operated experiments are however collected in Table 2.

**Tab.2:** Basic parameters of operated experiments.

Experiment #	Pressure / Oil p	Cell Assembly	Temperature / Power Input	Annotations
H 164	8 GPa / 280.6 bar	18/11	1600 °C / 1145.6 W	Coesite
H 166	8 GPa / 280.6 bar	18/11	1200 °C / 880.7 W	Densified Glass
H 167	8 GPa / 280.6 bar	18/11	800 °C / 603.8 W	Densified Glass
H 168	8 GPa / 280.6 bar	18/11	1500 °C / 1080.3 W	Coesite
H 170	8 GPa / 280.6 bar	18/11	1000 °C / 744 W	Densified Glass
H 171	20 GPa / 310 bar	10/4	RT / 0 W	4mm diameter rod machined down to 2.5 mm in diameter
H 173	8 GPa / 280.6 bar	18/11	1400 °C / 1013.8 W	Coesite

In Figure 9 the received samples are shown, whereat four samples (H166, H167, H170, H171) are clearly transparent and three of them (H164, H168, H173) are whitish with a polycrystalline matrix.

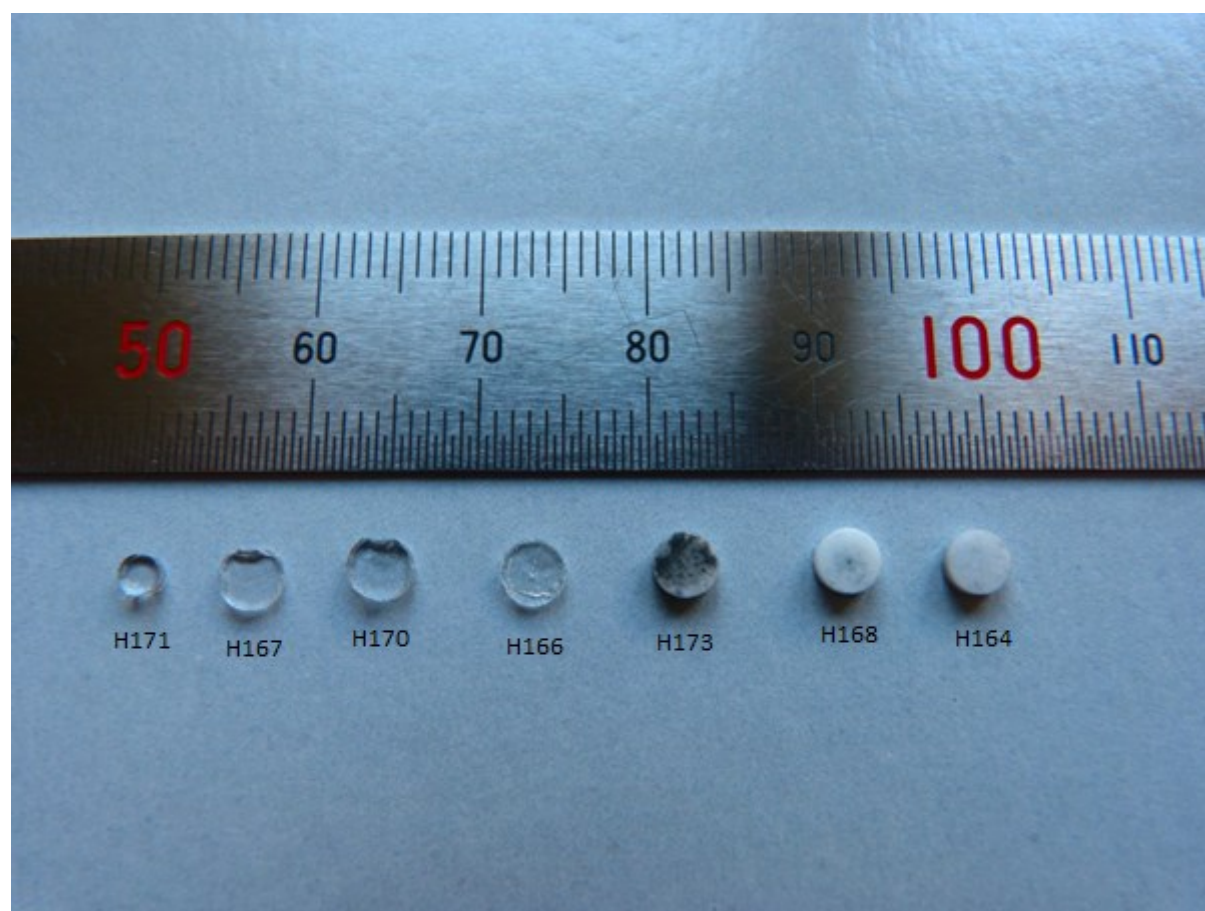


**Fig.9:** Synthesized samples with an increasing temperature input.

## 5. Results

### 5.1. XRD – Results

The X-ray diffraction patterns produced by XRD-measurements during this study show two distinct diagrams. In Figure 10 there are shown matching diffraction patterns of crystalline material, which is identified as pure coesite. This is expected due to the pure starting material and the pressure and temperature conditions of the known coesite stability field. Sample H173 synthesized at 8 GPa and 1400 °C however limps in respect due to intensity and presents between 25-30° an accumulation of peak positions, which is not shown within the diffraction patterns of sample H164 and H168.

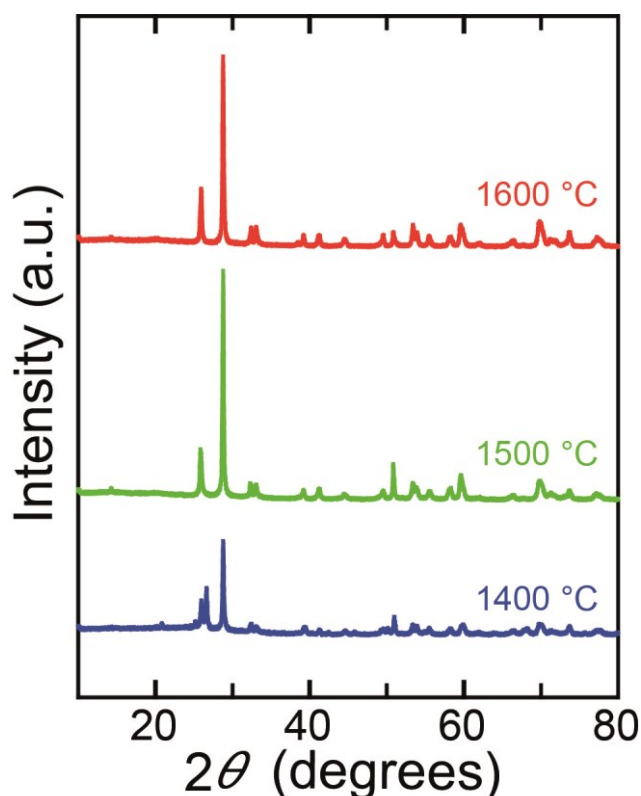


**Fig.10:** X-ray diffraction diagram of the samples H164, H168 & H173.

The samples H167, H170 and H166 with conditions of 8 GPa pressure output and an temperature input between 800 °C – 1200 °C as well as sample H171, which was synthesized under conditions of 20 GPa and ambient temperature, are showing a major difference in their diffraction pattern (Figure 11). These samples are amorphous and only show diffuse scattering. In Figure 11 also the diffraction pattern of the starting material was included for comparison. Thus a shifting of the broad diffraction peak to higher degrees including increasing peak intensity with increasing temperature from the starting material up to sample H166 can be determined.

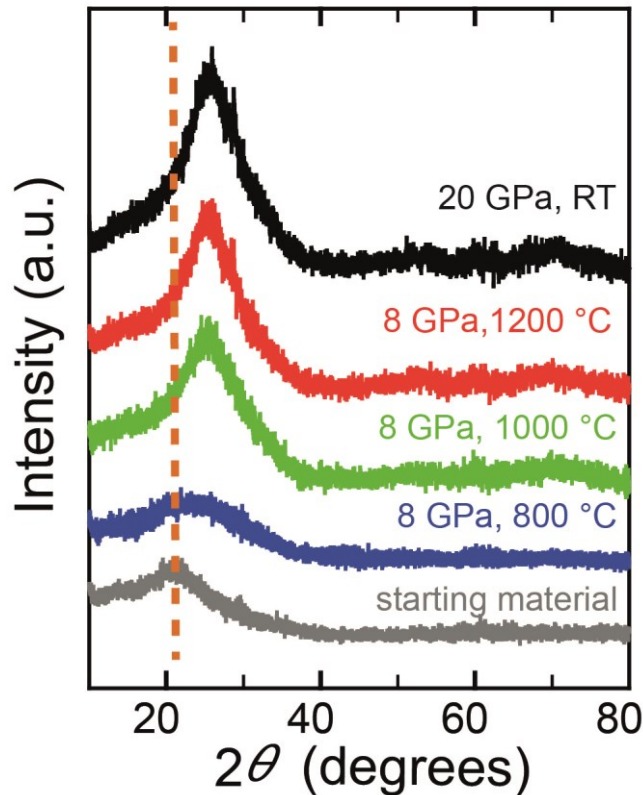


**Fig.11:** X-ray diffraction diagram of the samples H166, H167, H170, H171 and the starting material SK1310 for comparison.

## 5.2. Density Measurement Results

The density of the starting material is  $2.2 \text{ g/cm}^3$  given by its material master data sheet [1]. After the synthesis all the samples show a higher density, which is between  $2.6 \text{ g/cm}^3$  and  $3.0 \text{ g/cm}^3$ . In Figure 12 the dependence between density and the synthesis temperature of the samples was plotted. The interconnection shows an almost gradual increase of density with higher synthesis temperatures. Only sample H166 with a synthesis temperature of  $1200^\circ\text{C}$  presents a fairly lower value of density however within rather big error bars.

The highest value within this density dataset achieved the crystalline coesite sample H164 with a density of  $2.92 \text{ g/cm}^3$ . Zhou et al., 2005 as well as other authors report similar densities for the single crystal coesite likewise  $2.91\text{-}2.92 \text{ g/cm}^3$ . The crystalline samples H166 and H168 however possess a much lower density between  $2.72 \text{ g/cm}^3$  and  $2.86 \text{ g/cm}^3$ .

The amorphous silica with a synthesis temperature between  $800^\circ\text{C}$  and  $1200^\circ\text{C}$  possesses in comparison with the starting material also a much higher density between  $2.65 \text{ g/cm}^3$  and  $2.70 \text{ g/cm}^3$ . Therefore the synthesized amorphous silica samples can be characterized as densified silica glass.

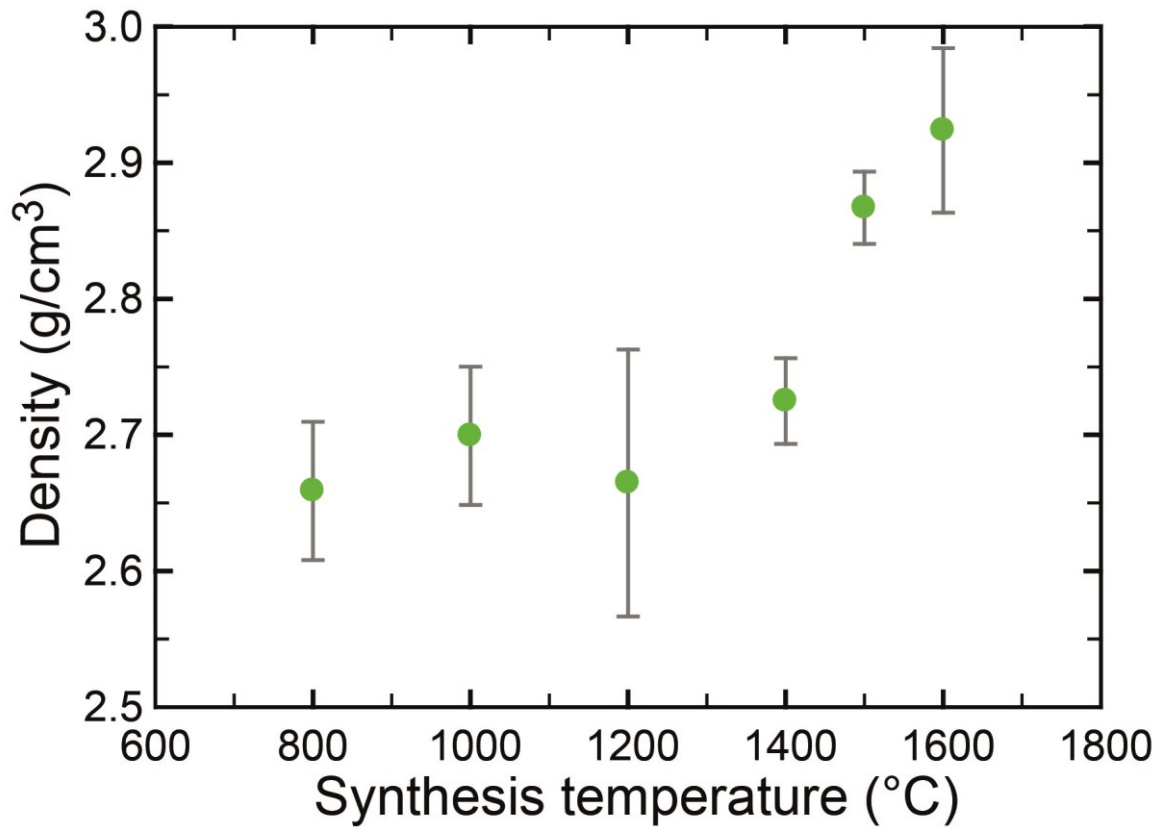


**Fig.12:** Diagram showing the interconnection between density and synthesis temperature of the samples H164, H166, H167, H168, H170 & H173.

### 5.3. Hardness Measurement Results

The Vickers hardness of the starting material is between 8.8-10.1 GPa given by its material master data sheet [1]. However the Vickers hardness could not be obtained for any of the synthesized samples during this study due to the only big indentation loads given within the experimental setup.

The Knoop hardness of the samples all lie in the same range between 8.25-8.73 GPa with a maximum of 0.86 deviation (Figure 13). Only sample H168 with the synthesis temperature of 1400 °C shows a distinct lower value with 6.45 GPa. This however cannot be taken as real hardness value due to the obvious brittle behavior of this sample. Therefore the hardness of the sample H166 could not be determined accurately. Also the samples H168 and H173 with synthesis temperatures of 1500 °C and 1400 °C showed brittle behavior during the hardness measurements, which is shown in Figure 14. These three crystalline samples are not well sintered and are therefore not reliable for the hardness study within this experimental series.



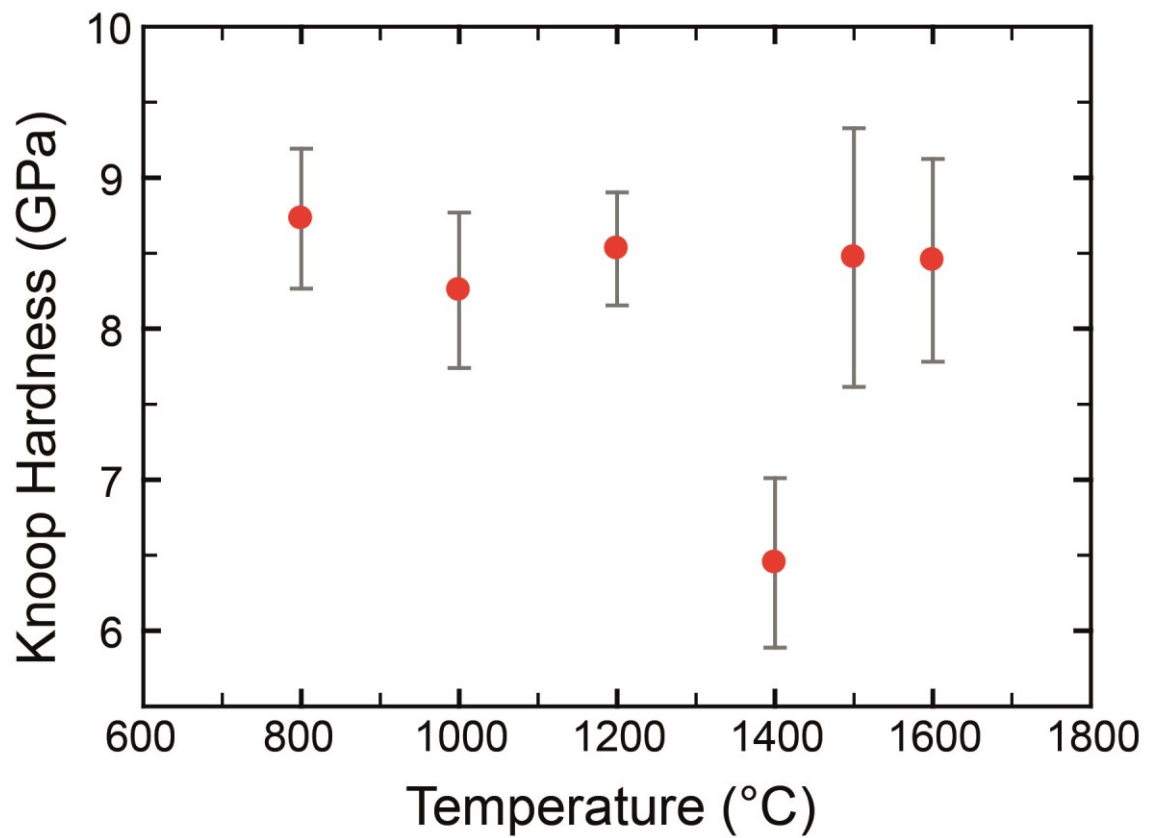


**Fig.13:** Diagram showing the interconnection between Knoop hardness and synthesis temperature of the samples H164, H166, H167, H168, H170 & H173.

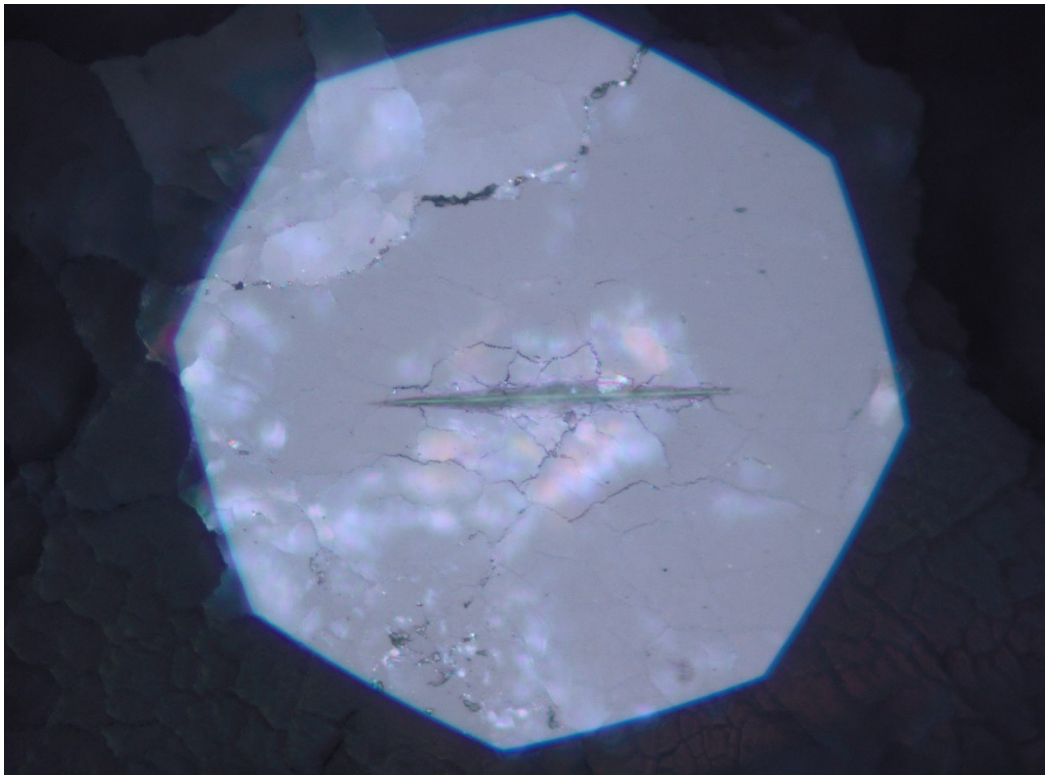


**Fig.14:** Picture showing the brittle behavior of sample H173.

#### 5.4. Toughness Measurement Results

No results about Vickers fracture toughness could be obtained due to the only big indentation loads given within the experimental setup. Knoop hardness tests are not giving any conclusion about the fracture toughness of a material.

### 6. Discussion

During this high pressure study an experimental series of samples under 8GPa and within a temperature range of 800 °C and 1600 °C was synthesized. These samples show a transition from densified SiO<sub>2</sub>-glass and the crystalline phase coesite.

The densified glass samples, which were synthesized at 8 GPa between 800 °C and 1200 °C, were completely transparent. Samples H166 and H170 however showed small crystalline patches on their original surface, which were removed during the measurement preparation polishing process. In general all three samples show a nice diffuse scattering within their XRD data and no distinct peaks, which presents totally amorphous samples. The density data shows a reliable average, however no trends are determinable. Almost the same is happening within the hardness data, which should also be reliable due to nice indentation traces.

The crystalline samples H164, H168 and H173 are not well sintered. They all show brittle behavior during hardness measurements. Sample H173 possesses the most obvious brittleness and fails almost completely any hardness test. This sample is as well eye catching within the plotted XRD data. This data shows a very low intensity in general and accumulates peaks at positions between 25-30° of 2θ, which could imply diffuse scattering whereat the background is not too noisy. This however would lead to the assumption of a heterogeneous sample with crystalline coesite and densified glass. The lower density of this sample would fit to this assumed material. Sample H168, which also shows a lower value in density as single crystal coesite, could therefore be a mixture of coesite and densified glass as well. The hardness data of the crystalline phases in general can't be related due to the unreliable measurements, but the brittle behavior would maybe explain these two phases within the bulk sample.



## References

- Anstis G.R., Chantikul P., Lawn B.R., Marshall D.B. (1981): A Critical Evaluation of Indentation Techniques for Measuring Fracture Toughness: I, Direct Crack Measurements. *Journal of the American Ceramic Society* 63, 533–538.
- Černok A., Ballaran T.B., Caracas R., Miyajima N., Bykova E., Prakapenka V., Liermann H.-P., Dubrovinsky L. (2014): Pressure-induced phase transitions in coesite. *American Mineralogist* 99, 755–763.
- Chao E.C.T., Shoemaker E.M., Madsen B.M. (1960): First natural occurrence of coesite. *Science* 132, 220–222.
- Chopin C. (1984): Coesite and pure pyrope in high-grade blueschists of the Western Alps: a first record and some consequences. *Contributions to Mineralogy and Petrology* 86, 107–118.
- Chuenarrom C., Benjakul P., Daosodsai P. (2009): Effect of Indentation Load and Time on Knoop and Vickers Microhardness Tests for Enamel and Dentin. *Materials Research* 12-4, 473–476.
- Coes L. (1953): A new dense crystalline silica. *Science* 118, 131–132.
- Cook R.F., Pharr G.M. (1990): Direct Observation and Analysis of Indentation Cracking in Glasses and Ceramics. In: *Journal of the American Ceramic Society* 73, 787–817.
- Frost D.J., Poe B.T., Trønnes R.G., Liebske C., Duba A., Rubie D.C. (2004): A new large-volume multianvil system. *Physics of the Earth and Planetary Interiors* 143–144, 507–514.
- Gaida N. (2014): Synthetic nanocrystalline composite ceramics – synthesis of tailored alternative materials of high pressure minerals. Master's Thesis.
- Parkinson C.D. (2000): Coesite inclusions and prograde compositional zonation of garnet in whiteschist of the HP-UHPM Kokchetav massif, Kazakhstan: a record of progressive UHP metamorphism. *Lithos* 52, 215–233.
- Smyth J., Hatton C. (1977) Coesite-sanidine grosspyrite from Roberts-Victor kimberlite. *Earth and Planetary Science Letters* 34, 284–290.
- Swamy V., Saxena S.K., Sundman B., Zhang J. (1994): A thermodynamic assessment of silica phase diagram. *Journal of Geophysical Research - Solid Earth* 99, 11787–11794.
- Walker D., Carpenter M.A., Hitch C.M. (1990): Some simplifications to multianvil devices for high pressure experiments. *American Mineralogist* 75, 1020–1028.
- Zhou Y., He C., Song J., Ma S., Ma J. (2005): An experiment study of quartz-coesite transition at differential stress. *Chinese Science Bulletin* 50-5, 446–451.

## Internet References

- [1] Material Master Data Sheet of SK1310 from OHARA Corporation:  
<http://www.oharacorp.com/pdf/SK1310.pdf>